2022 American Control Conference (ACC)
Atlanta, USA, June 8-10, 2022

# Scheduling Battery Energy Storage Systems Under Battery Capacity Degradation Uncertainty

Hannah Moring and Johanna L. Mathieu

***Abstract*— The increasing penetration of renewable energy resources and the decreasing cost of battery energy storage in recent years has led to a growing interest in using batteries to provide grid services like frequency regulation. In this paper, we discuss the advantages and disadvantages of different battery degradation models and the impacts that model choice can have on the assumed cost of energy capacity loss due to operation. We also explore the effects of modeling degradation as an uncertain process by extending a two-stage, multi-period optimization problem for scheduling the operation of a battery providing multiple services with risk aversion. We use stochastic dual dynamic programming to derive a policy for the problem. Case study results show that using a stochastic degradation model with risk aversion produces a policy for more conservative battery use and longer lifespan in comparison to that obtained with a deterministic degradation model.**

***Index Terms*— Battery Energy Storage, Capacity Degradation, Stochastic Dual Dynamic Programming, Degradation Uncertainty**

## NOMENCLATURE

### Sets and Indices

| | |
|---|---|
| $\mathcal{D}$ | Set of cycle depths $\delta$ realized during the time horizon, indexed by $i$. |
| $\mathcal{J}$ | Set of segments of the marginal cycle aging cost function with cardinality $J$, indexed by $j$. |
| $\mathcal{T}$ | Set of time intervals in the optimization horizon with cardinality $T$, indexed by $t$. |

### Parameters

| | |
|---|---|
| $a^{\mathrm{r}}$ | Flexible load nominal power consumption, kW. |
| $a^{\mathrm{l}}$, $a^{\mathrm{u}}$ | Flexible load lower, upper limit, kW. |
| $c^{\mathrm{b}}$ | Battery replacement cost, \$. |
| $E$ | Rated battery energy capacity, kWh. |
| $G$ | Line limit of the constrained line, kW. |
| $k$ | Penalty coefficient for increasing or decreasing the energy consumption of the flexible load, \$/kWh. |
| $\boldsymbol{m}$ | Vector $\in \mathbb{R}^J$ containing the slopes of the piecewise linear marginal cycle aging cost function, \$/kW. |
| $P$ | Battery power capacity, kW. |
| $\boldsymbol{s}_0^{\mathrm{b}}$ | Vector in $\mathbb{R}^J$ where element $j$ defines the initial energy level in battery segment $j$, kWh. |
| $s_0^{\mathrm{v}}$ | Flexible load virtual storage initial value, kWh. |
| $s^{\mathrm{v,l}}$ | Flexible load virtual storage lower limit, kWh. |
| $s^{\mathrm{v,u}}$ | Flexible load virtual storage upper limit, kWh. |
| $\alpha$ | CVaR confidence level, (-). |
| $\beta$ | Weight for CVaR, (-). |
| $\eta^{\mathrm{c}}$, $\eta^{\mathrm{d}}$ | Battery charging, discharging efficiency, %. |
| $\pi^{\mathrm{g}}$ | Price for buying/selling power, \$/kWh. |
| $\pi^{\mathrm{f}}$ | Price for providing frequency control, \$/kWh. |
| $\theta$ | Value at risk, (-). |

### Degradation Model Variables and Parameters

| | |
|---|---|
| $C_{\mathrm{c}}$ | Energy capacity loss due to calendar aging, %. |
| $C_{\mathrm{o}}$ | Energy capacity loss due to cycling, %. |
| $f$ | Number of equivalent full cycles, (-). |
| $n_i$ | Number of cycles of depth $\delta_i$, (-). |
| $s_i$ | Average state of charge of cycle depth $\delta_i$, (-). |
| $t^{\mathrm{m}}$ | Time, in months. |
| $T^{\mathrm{abs}}$ | Operating temperature, K. |
| $\delta_t, \delta_i$ | Cycle depth at time $t$, or indexed by $i$ (-) |
| $\Phi$ | Cycle depth stress for battery degradation, %. |

### State Variables

| | |
|---|---|
| $\boldsymbol{s}_t^{\mathrm{b}}$ | A vector $\in \mathbb{R}^J$ where element $j$ defines the energy level in battery segment $j$ at time $t$, kW. |
| $s_t^{\mathrm{b}}$ | Energy level in the battery, a scalar variable equal to $\mathbf{1}^\intercal \boldsymbol{s}_t^{\mathrm{b}}$, kW. |
| $s_t^{\mathrm{v}}$ | Virtual storage of flexible load, kWh. |

### Decision Variables

| | |
|---|---|
| $a_t$ | Power consumed by the flexible load, kW. |
| $b_t$ | Power allocated for frequency regulation, kW. |
| $c_t$ | Ratio of PV generation curtailed, (-). |
| $g_t$ | Power exchanged with the grid, kW. |
| $\boldsymbol{p}_t^{\mathrm{c}}$ | Vector $\in \mathbb{R}^J$ where element $j$ defines the power entering battery segment $j$ at time $t$, kW. |
| $\boldsymbol{p}_t^{\mathrm{d}}$ | Vector $\in \mathbb{R}^J$ where element $j$ defines the power leaving battery segment $j$ at time $t$, kW. |
| $p_t^{\mathrm{c}}$ | Power leaving the battery, a scalar variable equal to $\mathbf{1}^\intercal \boldsymbol{p}_t^{\mathrm{c}}$, kW. |
| $p_t^{\mathrm{d}}$ | Power leaving the battery, a scalar variable equal to $\mathbf{1}^\intercal \boldsymbol{p}_t^{\mathrm{d}}$, kW. |

### Stochastic Variables

| | |
|---|---|
| $\omega^{\mathrm{deg}}$ | Uncertain battery degradation model coefficient,(-). |
| $\omega_t^{\mathrm{f}}$ | Frequency regulation signal, (-). |
| $\omega_t^{\mathrm{pv}}$ | PV system output, kW. |

This work was supported by NSF Grant 1845093. The authors are with the Department of Electrical Engineering and Computer Science, University of Michigan, Ann Arbor, MI, USA {hmoring, jlmath}@umich.edu

## I. INTRODUCTION

Decreasing costs of batteries and increasing penetration levels of intermittent renewable energy sources have led to an increased use of battery energy storage to maintain robustness and resiliency in power systems [1]. However, the current costs, economical and environmental, of batteries hinder their wide-spread use. Extending the cycle life of a battery, the length of time until a battery reaches its end of life (EOL), through mindful operation can lower its

978-1-6654-5196-3/$31.00 ©2022 AACC

equivalent annual cost. EOL is typically defined as 20% loss of rated energy capacity [2], [3].

How batteries are operated affects how they degrade, or how their usable storage capacity decreases. Battery degradation is a nonlinear function of environmental and operating parameters, making it challenging to model accurately [4]. Omitting or inaccurately modelling degradation can lead to undesirable capacity loss, necessitating more frequent replacement. This increases both the economic and environmental costs. Accurate models are complex and require extensive operational data. Different battery chemistries have different degradation dynamics. Moreover, a degradation model developed for one battery may describe the degradation of another battery of the same type and size poorly because of differences in manufacturing, ambient conditions, and so on [5], [6].

In this paper, we propose a new approach to schedule a battery energy storage system (BESS) to provide multiple grid services while accounting for capacity degradation. In particular, motivated by the difficulty of accurately capturing battery degradation processes, we propose a stochastic model for battery degradation and show how it can be incorporated into a stochastic dual dynamic programming (SDDP) formulation that optimizes the operation of a BESS simultaneously managing the power flow along a constrained line and providing frequency regulation to the bulk network. We use the conditional value at risk ($\text{CVaR}_\alpha$) as a means to minimize the risk of considerable battery degradation. For a given $\alpha \in (0,1)$, $\text{CVaR}_\alpha$ is defined as the expected value of the cost greater than the $(1-\alpha)$-quantile of the cost distribution [7], [8]. In the context of our problem, this is the expected cost of degradation for the $\alpha$-fraction of most expensive degradation.

Researchers have developed algorithms to optimize the use of BESS providing grid services to maximize revenue, accounting for different types of services and degradation [1], [9]–[12]. However, this prior work has used deterministic degradation models. In [9], degradation is modeled as a near-quadratic cycle depth stress function, where cycle depth and duplicity are found using an approximation of the rainflow method. The rainflow counting algorithm was originally derived for material stress analysis under cyclical loading, but has been applied to batteries to find incremental degradation due to cycling in recent years. In [10], capacity degradation is modeled as a non-linear function of average state of charge (SOC), cycle depth, and number of cycles derived from accelerated cycle ageing tests. A kinetic battery model for lead acid batteries was extended to other battery chemistries and linearized in [12]. Another method for accounting for degradation that has been used in optimization problems is to limit the SOC to a given range where degradation tends to be less severe and assigning a constant marginal cost for charging and discharging, as in [1], [11]. All of the aforementioned degradation models have advantages and disadvantages with regard to accuracy and computational expense. The use of different models may lead to different optimal solutions for problems that otherwise have the same formulation, and inaccuracy in the degradation model will lead to sub-optimal operation [4]. This points to the need to carefully understand the impact that our choice of degradation model has on solutions and the need to explicitly capture model uncertainty in our formulations.

There are four main contributions of this paper. First, we provide a comparison of three degradation models, and discuss how their different degradation magnitudes and dynamics could affect solutions. Second, we develop a stochastic degradation model based on the deterministic model in [9]. Third, we develop an SDDP approach to optimize BESS operation subject to our stochastic degradation model. The optimization formulation is an extension of that in [11], which used a simpler, deterministic degradation model. Finally, we demonstrate the approach through a case study and discuss the impacts of modeling degradation as a stochastic process in BESS operation optimization problems.

The remainder of this paper is organized as follows. Section II motivates the modeling of capacity degradation as a stochastic process. In Section III, we develop the stochastic battery degradation model and the SDDP problem formulation. Section IV presents and discusses results from a case study. Conclusions are presented in Section V.

## II. Motivation for Modeling Degradation as a Stochastic Process

Electrochemical models are the most accurate types of models for capturing battery dynamics and aging [13]. Electrochemical models of lithium ion (Li-ion) batteries incorporate constitutive laws to describe Li-ion transportation, which requires detailed information about the battery's geometry and chemical properties, as well as extensive laboratory testing [2]. Electrochemical models are generally non-convex, making them computationally intractable to implement with many optimization algorithms commonly used in the power systems domain.

Due to the complexities and computational difficulties associated with electrochemical models, many simplified battery aging models have been developed to be used in optimization formulations [3], [14]. These simplified models represent degradation as a function of one or more of the following parameters: time, number of cycles, state of charge, cycle depth, temperature, and rate of charge/discharge. The computational advantages of these models come at a cost of accuracy [2].

To highlight how the choice of degradation model can affect the modeled capacity loss from operation, we compare three degradation models for a Li-ion battery. The comparison is made by simulating a battery following the PJM dynamic frequency regulation (FR) signal (RegD) obtained from [15] over the course of a day. For simplicity, we assume that the battery follows the same daily trajectory for 10 years. Due to the random nature of FR signals, this assumption would not hold in practice. However, we would expect trajectories to have similar overall characteristics day to day, and so do not expect that this simplifying assumption has a large impact on the overall results. This method ignores

the downward trend in SOC overtime due to battery losses and the energy injections required to increase the SOC.

The three models used are from [9], [10], [13] and will be referred to by their citation number. Each model has two components: a calendar aging component $C_{\mathrm{c}}$ and a cycling aging component $C_{\mathrm{o}}$. Both components represent energy capacity degradation as a percentage of the rated energy capacity. The two components are calculated separately and summed to get the total energy capacity loss.

The model from [9] uses the rainflow counting algorithm with an incremental cycle depth stress function to calculate degradation. The calendar component is given as a constant annual capacity degradation of $C_{\mathrm{c}} = 2\%$. The cycling component is

$$C_{\mathrm{o}} = \sum_{\delta_i \in \mathcal{D}} 1.048 \times 10^{-2} \delta_i^{2.03}, \tag{1}$$

where $\mathcal{D}$ is the set of all cycle depths $\delta_i$ realized during the time horizon. Note that in [9], degradation is given as a percentage of battery life, and so $C_{\mathrm{o}} = 100\%$ equates to 20% loss of rated energy capacity (i.e., EOL is at 80% battery capacity). However, here we wish to capture to the entire capacity of the battery so we adjust the coefficient in (1) so that $C_{\mathrm{o}} = 20\%$ equates to 20% loss of rated energy capacity.

The model from [10] also utilizes the rainflow counting algorithm, but with calendar and cycling components

$$C_{\mathrm{c}} = 0.1723 e^{0.007388 s} (t^{\mathrm{m}})^{0.8}, \tag{2}$$

$$C_{\mathrm{o}} = \sum_{\delta_i \in \mathcal{D}} 0.021 e^{-0.01943 s_i} \delta_i^{0.7162} (n_i)^{0.5}, \tag{3}$$

where $s_i$ is the average state of charge of cycle depth $\delta_i$, $t^{\mathrm{m}}$ is the time in months, and $n_i$ is the number of cycles of depth $\delta_i$.

The model from [13] is an equivalent electrical circuit model developed from accelerated calendar and cycle testing. The calendar component $C_{\mathrm{c}}$ and cycling component $C_{\mathrm{o}}$ of the model are

$$C_{\mathrm{c}} = 3.087 \times 10^{-7} e^{0.05146 T^{\mathrm{abs}}} (t^{\mathrm{m}})^{0.5}, \tag{4}$$

$$C_{\mathrm{o}} = 6.87 \times 10^{-5} e^{0.027 T^{\mathrm{abs}}} f^{0.5}, \tag{5}$$

where $T^{\mathrm{abs}}$ is the temperature in Kelvin, $t^m$ is the time in months, and $f$ is the number of equivalent full cycles.

We assume an operating temperature of $25°C$ $(298.15K)$. We use the rainflow method to extract the cycle depths, as well as the corresponding duplicity and average SOC for each cycle depth [9]. The number of equivalent full cycles is calculated as the total energy throughput divided by the rated energy capacity. The parameters required by each model are then used to calculate degradation.

Fig. 1 shows the estimated capacity degradation for each of the three models resulting from operating a battery following the same FR signal for 10 years. The cycle life is 2.56 years for the model in [9], 5.01 years for the model in [10], and 3.82 years for the model in [13]. The variation in estimated battery life and degradation dynamics given by these three models resulting from the same operating scheme suggests that the choice of degradation model has an impact on the estimated operating cost caused by energy capacity loss.

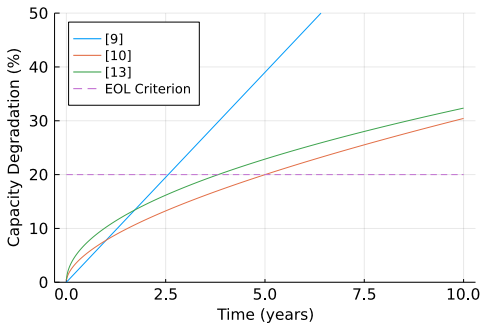


Fig. 1. Comparison of capacity degradation for a simulated battery calculated from three models used in BESS operation optimization problems.

In summary, different models lead to significantly different calculated values of degradation for the same operating conditions. In the next section, we will investigate the impact of accounting for degradation model inaccuracy in a BESS operation optimization problem by modeling degradation as a uncertainty process.

## III. Problem Description

We consider the system depicted in Fig. 2 and a modified version of the problem presented in [11]. The system is composed of a BESS, a flexible load, and a photovoltaic (PV) system which are connected to the grid by a constrained line. The BESS is primarily used to manage the line constraint but the BESS operator also wants to sell unused capacity for FR to offset its costs, while considering the cost of degradation. The choice of FR capacity must be made in advance of real-time operation. In addition to the BESS, the PV system and the load are controllable. Specifically, the PV system's power output can be reduced. The load is permitted to vary within a range but it is desired that it maintain a baseline. The limited, time-integrated difference between the baseline and the actual consumption of the load is modeled as virtual storage.

While the basic setup described above is similar to that in [11], our formulation has five key differences. To better represent US markets, we consider one FR service while two are considered in [11]. We model the FR signal on the real 2-second time interval, whereas it is modeled as a 5-minute moving average in [11]. Our method allows for more accurate modeling of BESS dynamics. In our model, the curtailment ratio, power allocated to the flexible load, and power into or out of the BESS are decided after the PV output and FR signal are realized. This is differs from the formulation in [11], where all decision variables, except the power into and out of the BESS, are chosen before knowing the PV output and FR signal. In [11], the cost of degradation is approximated as a deterministic quadratic function of the energy level deviation from a desired level. In contrast, here we use the more detailed degradation model from [9], and extend it to a stochastic model by treating a key parameter as

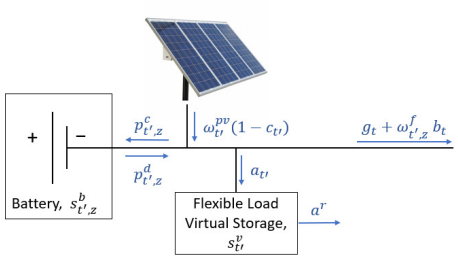


Fig. 2. Diagram of system in which a BESS and flexible load manage a grid constraint given uncertain solar PV production.

uncertain. Finally, our formulation incorporates risk aversion, which was not considered in [11].

In summary, our objective is to develop a policy to minimize the expected operational costs and the risk of significant degradation of the BESS under uncertainty in the PV power output, the FR signal, and the degradation model. We must commit in advance to the FR power capacity and net power exchanged with the grid (i.e., how much energy is bought/sold in the energy market) every 5 min for the next 12 hours, and are able to adjust the BESS power, PV curtailment, and flexible load consumption in real-time after uncertainty is revealed according to our control policy.

### A. Stochastic Dual Dynamic Programming

We solve our problem using SDDP, a methodology for solving convex, multistage, stochastic programs [16]. Stochastic dynamic programming (SDP) is the typical method for solving multistage, stochastic programs, which are not necessarily convex. However, SDP requires discretization of the action space, state space, and stochastic variable space, which makes it computationally expensive for large problems, e.g., as shown in [11]. We chose to use SDDP because it only requires discretization of the stochastic variable space. While SDDP extensions addressing some types of nonconvexities do exist e.g., [17], here we consider only convex problems, as further discussed in Section III-D.

In SDDP, variables are defined as either a state, decision, or stochastic variable. A state variable represents information required at the present time and onward and/or in subsequent stages. A decision variable represents a decision made within a stage or time period. A stochastic variable is a stage-wise independent random variable [14]. SDDP approximates the expected cost-to-go function with piecewise linear functions obtained from the dual solutions of the optimization problem at each stage.

The algorithm has two components: the forward pass where scenarios are sampled based on the probability distribution of the random variables, and the backward pass where each stage is optimized along the sampled trajectory from the forward pass in reverse order. In the backward pass, a Bender's cut is added to improve the approximation of the expected cost-to-go function using the Lagrange multipliers from the optimized stage problem. This sequence of forward and backward passes is repeated until some specified stopping criteria is reached. A lower bound is obtained from the solution of the first stage problem and an upper bound can be approximated from a Monte Carlo simulation of the policy [18], [16]. Note that this upper bound is a confidence interval.

### B. Stochastic Degradation Model

Many battery degradation models are non-convex, making them incompatible with traditional SDDP approaches. The model presented in [9] is convex and closely approximates the rainflow counting method, which has been used extensively in literature to model battery degradation [14], [13], [19]. For this reason, we derived our stochastic degradation model from that model.

In [9], the incremental cycle aging is given by a cycle depth stress function $\Phi(\delta_t)$, where $\delta_t$ is the cycle depth at time $t$, defined as

$$\delta_t = \frac{p_t^{\mathrm{d}} \Delta t}{\eta^{\mathrm{d}} E}, \tag{6}$$

where $p_t^{\mathrm{d}}$ is the power discharged at time step $t$ of duration $\Delta t$, $\eta^{\mathrm{d}}$ is the discharge efficiency, and $E$ is the rated capacity of the battery. The marginal cycle aging for a particular cycle depth $\delta_i$ is given by [9]

$$\frac{\partial \Phi(\delta_i)}{\partial p_i^{\mathrm{d}}} = \frac{d\Phi(\delta_i)}{d\delta_i}\frac{\partial \delta_i}{\partial p_i^{\mathrm{d}}} = \frac{\Delta t}{\eta^{\mathrm{d}} E}\frac{d\Phi(\delta_i)}{d\delta_i}, \tag{7}$$

where $p_i^{\mathrm{d}}$ is the power discharged from the battery over $\Delta t$ resulting in cycle depth $\delta_i$. If $\Phi(\delta_t)$ is a convex function, then the marginal cycle aging (7) can be upper-bound approximated by a piecewise linear function of $J$ segments, indexed by $j$. Each segment $j$ corresponds to a range of cycle depths $\delta \in [\frac{j-1}{J}, \frac{j}{J})$. The slope of segment $j$ is

$$m_j = \frac{\Delta t}{\eta^{\mathrm{d}} E} J \left( \Phi\left(\frac{j}{J}\right) - \Phi\left(\frac{j-1}{J}\right)\right), \forall j = 1, ..., J. \tag{8}$$

Denote $\boldsymbol{m} \in \mathbb{R}^J$ as the vector of all $m_j$. This approximation allows degradation costs to vary as a function of cycle depth, with larger cycle depths having higher costs.

The cycle depth stress function, $\Phi(\delta_t)$, is empirically derived from tests conducted by repeatedly cycling a battery through a specified series of cycle depths or SOC trajectory and has some level of inaccuracy [20]. The function presented in [9] is given as

$$\Phi(\delta_t) = (5.24 \times 10^{-4})\delta_t^{2.03}. \tag{9}$$

Here, we propose to replace the deterministic coefficient $5.24 \times 10^{-4}$ with a stochastic coefficient $\omega^{\mathrm{deg}}$ that takes values from a discrete set $\Omega^{\mathrm{deg}}$. Equation (8) can then be rewritten as

$$m_j = \frac{\Delta t}{\eta^{\mathrm{d}} E} J \left( \omega^{\mathrm{deg}} \left(\frac{j}{J}\right)^{2.03} - \omega^{\mathrm{deg}} \left(\frac{j-1}{J}\right)^{2.03}\right). \tag{10}$$

This can be further decomposed as

$$m_j = \omega^{\mathrm{deg}} m_j^*, \tag{11}$$

where

$$m_j^* = \frac{\Delta t}{\eta^{\mathrm{d}} E} J \left( \left( \frac{j}{J} \right)^{2.03} - \left( \frac{j-1}{J} \right)^{2.03} \right). \tag{12}$$

This decomposition makes it possible to model $\omega^{\mathrm{deg}}$ as a stochastic variable in the optimization problem while keeping $m_j^*$ as a separate auxiliary variable. Denote $\boldsymbol{m}^* \in \mathbb{R}^J$ as the vector of all $m_j^*$.

### C. Formulation

We formulate a two-stage, multi-period problem to decide how much energy is bought from or sold to the grid $g_t$ (kW) and how much of the BESS's power capacity is allocated to FR $b_t$ (kW) in each time step $t \in \mathcal{T}$ of duration $\Delta t$ for the next $T$ time steps. These decisions are made before the PV power output and FR signal are known and make up the first stage decisions, which are committed for the entire time horizon. We assume that once these commitments have been made, they are fulfilled. These variables are both control variables and state variables because they represent decisions in the first stage and information needed in the second stage.

We use $t'$ to denote time $t$ in the second stage (i.e., after uncertainty is revealed) and $z$ to denote the 2-second subinterval on which the FR signal, BESS power, and SOC update. The second stage decisions are the PV curtailment ratio $c_{t'}$ (-), power allocated to the flexible load $a_{t'}$ (kW), and power into $p^{\mathrm{c}}_{t',z}$ (kW) or out of $p^{\mathrm{d}}_{t',z}$ (kW) the BESS. They are made with knowledge of the first stage decisions, the PV power output, the FR signal, and the degradation model coefficient. To use the degradation model from Section III-B, we segment the BESS's energy level $s^{\mathrm{b}}$, $p^{\mathrm{c}}$, and $p^{\mathrm{d}}$ each into $J$ segments indexed by $j$, as explained in [9]. The segmented vectors are denoted $\mathbf{s}^{\mathrm{b}} \in \mathbb{R}^J$, $\mathbf{p}^{\mathrm{c}} \in \mathbb{R}^J$, and $\mathbf{p}^{\mathrm{d}} \in \mathbb{R}^J$, respectively. The sum of the elements of each vector equals the total quantity, i.e., $s^{\mathrm{b}} = \mathbf{1}^\intercal \mathbf{s}^{\mathrm{b}}$, $p^{\mathrm{c}} = \mathbf{1}^\intercal \mathbf{p}^{\mathrm{c}}$, and $p^{\mathrm{d}} = \mathbf{1}^\intercal \mathbf{p}^{\mathrm{d}}$. Then, we treat the vectors $\mathbf{p}^{\mathrm{c}}_{t',z}$ and $\mathbf{p}^{\mathrm{d}}_{t',z}$ as second stage decisions.

The stochastic variables are the degradation model coefficient $\omega^{\mathrm{deg}}$ (-), the PV system output $\omega^{\mathrm{pv}}_{t'}$ (kW), and the FR signal $\omega^{\mathrm{f}}_{t',z}$ (-). The state variables are the energy level of the BESS $s^{\mathrm{b}}_{t'}$ (kWh) and the virtual storage level of the flexible load $s^{\mathrm{v}}_{t'}$ (kWh).

In summary, the first stage action vector is $\boldsymbol{x}_t = [g_t \quad b_t]^\intercal$, the second stage action vector is $\boldsymbol{x}_{t',z} = [\boldsymbol{p}^{\mathrm{c}}_{t',z}{}^\intercal \quad \boldsymbol{p}^{\mathrm{d}}_{t',z}{}^\intercal \quad c_{t'} \quad a_{t'}]^\intercal$, the stochastic variable vector is $\boldsymbol{\omega}_{t',z} = [\omega^{\mathrm{deg}} \quad \omega^{\mathrm{pv}}_{t'} \quad \omega^{\mathrm{f}}_{t',z}]^\intercal$, and the state vector is $\boldsymbol{s}_{t',z} = [\boldsymbol{s}^{\mathrm{b}}_{t',z}{}^\intercal \quad s^{\mathrm{v}}_{t'}]^\intercal$.

The cost function for the first stage is

$$\min_{\boldsymbol{x}} C_1 + (1-\beta)\,\mathbb{E}[C_2] + \beta \mathrm{CVaR}_\alpha(\boldsymbol{x}_{t',z}), \tag{13}$$

where $C_1$ is the cost associated with the first stage decisions, $C_2$ is the cost associated with second stage decisions, $\mathrm{CVaR}_\alpha$ is a risk measure on degradation, and $\beta \in [0,1]$ is a weight. Specifically, the first stage cost function is

$$C_1(\boldsymbol{x}_t) = \sum_{t \in \mathcal{T}} \Delta t(-\pi^{\mathrm{g}} g_t - \pi^{\mathrm{f}} b_t), \tag{14}$$

where $\pi^{\mathrm{g}}$ is the price for power bought from or sold to the grid (\$/kWh) and $\pi^{\mathrm{f}}$ is the price for FR power capacity (\$/kWh). We assume that all offered capacity is procured by the system operator, which is reasonable if storage offers capacity at low cost. The second stage cost is

$$C_2(\boldsymbol{x}_t, \boldsymbol{x}_{t',z}, \boldsymbol{\omega}_{t',z}, \boldsymbol{s}_{t',z}) = \sum_{t \in \mathcal{T}} \Delta t(k(s^{\mathrm{v}}_{t'})^2 + C^{\mathrm{bat}}_{t',z}), \tag{15}$$

where $k$ is a penalty coefficient for increasing or decreasing the energy consumption of the flexible load and $C^{\mathrm{bat}}_{t',z}$ is the marginal cost of cycle aging for the BESS, i.e.,

$$C^{\mathrm{bat}}_{t',z} = \frac{1}{2} c^{\mathrm{b}} \omega^{\mathrm{deg}} \boldsymbol{m}^{*\intercal} (\boldsymbol{p}^{\mathrm{c}}_{t',z} + \boldsymbol{p}^{\mathrm{d}}_{t',z}), \tag{16}$$

where $c^{\mathrm{b}}$ is the replacement cost of the BESS (\$). For a discrete distribution, $\mathrm{CVaR}_\alpha(\boldsymbol{x}_{t',z})$ is defined in [7] $\forall \alpha \in (0,1)$ as

$$\mathrm{CVaR}_\alpha(\boldsymbol{x}_{t',z}) = \max \left\{ \theta - \frac{1}{1-\alpha} \mathbb{E}\left[\max\{\theta - C_2, 0\}\right] \right\}, \tag{17}$$

where $\theta$ is the value-at-risk. We also note that the second stage cost function is $\min_{\boldsymbol{x}} C_2(\boldsymbol{x}_t, \boldsymbol{x}_{t',z}, \boldsymbol{\omega}_{t',z}, \boldsymbol{s}_{t',z})$.

Both stage problems are subject to the following constraints. The power capacity allocated to frequency regulation must be non-negative,

$$b_t \geq 0, \qquad \forall t \in \mathcal{T}. \tag{18}$$

For any realization of the frequency regulation signal, the power exchanged with the grid must be within the line limit,

$$g_t + b_t \leq G, \qquad \forall t \in \mathcal{T}, \tag{19}$$

$$g_t - b_t \geq -G, \qquad \forall t \in \mathcal{T}, \tag{20}$$

where $G$ is the line limit. The curtailment ratio is limited

$$0 \leq c_{t'} \leq 1, \qquad \forall t' \in \mathcal{T}, \tag{21}$$

and the power allocated to the flexible load must remain within the range $[a^{\mathrm{l}}, a^{\mathrm{u}}]$,

$$a^{\mathrm{l}} \leq a_{t'} \leq a^{\mathrm{u}}, \qquad \forall t' \in \mathcal{T}. \tag{22}$$

The power constraints on the BESS are

$$p^{\mathrm{c}}_{t',z} = \sum_{j \in \mathcal{J}} p^{\mathrm{c}}_{t',z,j}, \qquad \forall t' \in \mathcal{T},\ \forall z \in \mathcal{Z}, \tag{23}$$

$$p^{\mathrm{d}}_{t',z} = \sum_{j \in \mathcal{J}} p^{\mathrm{d}}_{t',z,j}, \qquad \forall t' \in \mathcal{T},\ \forall z \in \mathcal{Z}, \tag{24}$$

$$0 \leq p^{\mathrm{c}}_{t',z} \leq P B_{t',z}, \qquad \forall t' \in \mathcal{T},\ \forall z \in \mathcal{Z}, \tag{25}$$

$$0 \leq p^{\mathrm{d}}_{t',z} \leq P(1 - B_{t',z}), \qquad \forall t' \in \mathcal{T},\ \forall z \in \mathcal{Z}, \tag{26}$$

$$0 \leq B_{t',z} \leq 1, \qquad B_{t',z} \in \mathbb{Z},\ \forall t' \in \mathcal{T},\ \forall z \in \mathcal{Z}, \tag{27}$$

where $P$ is the BESS power capacity and $B_{t',z}$ is a binary variable equal to 1 if the BESS is charging and 0 if the BESS

is discharging, which is used to prevent simultaneous charging and discharging. The net power entering the BESS is a function of the first stage decisions, uncertainty realizations, and the other second stage decisions,

$$p^{\mathrm{c}}_{t',z} - p^{\mathrm{d}}_{t',z} = \omega^{\mathrm{pv}}_{t'}(1 - c_{t'}) - \omega^{\mathrm{f}}_{t',z} b_t - g_t - a_{t'}, \quad \forall t' \in \mathcal{T},\ \forall z \in \mathcal{Z}. \tag{28}$$

The energy constraints on the BESS are

$$0 \le s^{\mathrm{b}}_{t',z,j} \le E/J, \qquad \forall t' \in \mathcal{T},\ \forall z \in \mathcal{Z},\ \forall j \in \mathcal{J}, \tag{29}$$

$$\boldsymbol{s}^{\mathrm{b}}_{1,1} = \boldsymbol{s}^{\mathrm{b}}_0, \tag{30}$$

$$\sum_{j \in \mathrm{J}} \boldsymbol{s}^{\mathrm{b}}_{T,Z,j} = \sum_{j \in \mathrm{J}} \boldsymbol{s}^{\mathrm{b}}_{0,j}. \tag{31}$$

where (29) limits the energy in each energy level segment to the rated energy capacity divided by the number of segments, (30) sets the initial energy levels in each segment to the known levels $\boldsymbol{s}^{\mathrm{b}}_0$, and (31) requires that the total energy in the BESS at the beginning and end of the horizon is the same. The energy level evolution for each segment is determined with the vector equations

$$\boldsymbol{s}^{\mathrm{b}}_{t',1} = \boldsymbol{s}^{\mathrm{b}}_{t'-1,Z} + \Delta t(\eta^c \boldsymbol{p}^{\mathrm{c}}_{t',1} - \boldsymbol{p}^{\mathrm{d}}_{t',1}/\eta^{\mathrm{d}}), \quad \forall t' \in \mathcal{T} \setminus 1. \tag{32}$$

$$\boldsymbol{s}^{\mathrm{b}}_{t',z} = \boldsymbol{s}^{\mathrm{b}}_{t',z-1} + \Delta t(\eta^c \boldsymbol{p}^{\mathrm{c}}_{t',z} - \boldsymbol{p}^{\mathrm{d}}_{t',z}/\eta^{\mathrm{d}}), \quad \forall t' \in \mathcal{T},\ \forall z \in \mathcal{Z} \setminus 1. \tag{33}$$

where $\eta^{\mathrm{c}}$ is the charging efficiency and $\eta^{\mathrm{d}}$ is the discharging efficiency.

The constraints defining the virtual storage level of the flexible load are

$$s^{\mathrm{v}}_1 = s^{\mathrm{v}}_0, \tag{34}$$

$$s^{\mathrm{v,l}} \le s^{\mathrm{v}}_{t'} \le s^{\mathrm{v,u}}, \tag{35}$$

$$s^{\mathrm{v}}_{t'} = s^{\mathrm{v}}_{t'-1} + \Delta t(a_{t'} - a^{\mathrm{r}}), \qquad \forall t' \in \mathcal{T} \setminus 1. \tag{36}$$

where (34) sets the initial energy level to the known level $s^{\mathrm{v}}_0$ and (35) limits the virtual storage level. Equation (36) computes the changes in the virtual storage level over time, where $a^{\mathrm{r}}_{t'}$ is the nominal power consumption of the load.

### D. Convex Relaxation

The traditional SDDP approach is only applicable to convex problems. Constraints (25)-(27) make our problem nonconvex. While extensions of SDDP for solving nonconvex problems exist, they generally lead to significant increases in problem size. For example, stochastic dual dynamic integer programming, presented in [17], requires a binary expansion of the state variables. For computational tractability, we chose to relax the binary constraint in our formulation rather than implement a method compatible with nonconvex SDDP formulations.

Removing (27) and replacing (25)-(26) with

$$0 \le p^{\mathrm{c}}_{t',z} \le P, \qquad \forall t \in \mathcal{T},\ \forall z \in \mathcal{Z}, \tag{37}$$

$$0 \le p^{\mathrm{d}}_{t',z} \le P, \qquad \forall t \in \mathcal{T},\ \forall z \in \mathcal{Z}, \tag{38}$$

TABLE I
CASE STUDY PARAMETERS

| Parameter | Value (unit) |
|---|---|
| $T$, $Z$, $J$ | 144, 150, 10 (-) |
| $\Delta t$, $\Delta z$ | 0.0833, 8.4745E-5 (hour) |
| $\pi^{\mathrm{g}}$, $\pi^{\mathrm{f}}$ | 0.20, 0.03 ($/kWh) |
| $E$ | 1600 (kWh) |
| $P$, $G$ | 600, 400 (kW) |
| $a^{\mathrm{l}}$, $a^{\mathrm{r}}$, $a^{\mathrm{u}}$ | 100, 200, 300 (kW) |
| $\eta^{\mathrm{d}}$, $\eta^{\mathrm{c}}$ | 0.95, 0.95 (-) |
| $s^{\mathrm{v,l}}$, $s^{\mathrm{v}}_0$, $s^{\mathrm{v,u}}$ | -400, 0, 400 (kWh) |
| $c^{\mathrm{b}}$ | 300 ($/kWh) |
| $k$ | 0.004 ($\mathrm{kW}^{-2}\mathrm{h}^{-3}$) |
| $s^{\mathrm{b}}_0$ | 800 (kWh) |
| $\beta$, $\alpha$ | 0.5, 0.25 (-) |

results in a convex formulation of our problem. Relaxing these constraints permits simultaneous charging and discharging by the BESS. While simultaneous charging and discharging may not physically feasible (and is certainly not desirable), mathematically it acts a way to remove energy from the system as energy losses due to inefficiency. Constraints (25)-(26) are inactivate unless there is benefit in removing energy from the system. In our model, the cost of degradation is modeled as a function of charge and discharge power, giving an inherent cost to energy losses. For this reason, we expect the optimal solution of the convex formulation would rarely choose to simultaneously charge and discharge. We verify this in the following section.

## IV. CASE STUDY

This section presents the results from a case study using the parameters shown in Table I. The initial BESS energy level $s^{\mathrm{b}}_0 = 800$ kWh is allocated to the energy level segments by "filling" the segments in ascending order by index number until the sum of segment-wise energy levels equals the total energy level. The time horizon is 12 hours corresponding to the middle of the day. We use 16 scenarios for PV power output and FR signal. We used historical data from NREL for PV generation in Michigan during July 2006 [21], which is given in 5-min time steps. The FR signal used was the RegD signal from PJM for July 2020 [15], which is given in 2-second time steps. We defined the set of possible stochastic degradation coefficients $\Omega^{\mathrm{deg}}$ to be the normally distributed set of 20 evenly spaced values in $[1.81 \times 10^{-5}, 1.03 \times 10^{-3}]$. This gives $\Omega^{\mathrm{deg}}$ a mean of $5.24 \times 10^{-4}$, the coefficient given in [9].

To analyze the effects that modeling degradation as a stochastic process has on the policy obtained by SDDP for our formulation, we also simulated a formulation of our problem with a deterministic degradation model for comparison. The deterministic degradation model formulation is identical to the formulation outlined in Section III except $\omega^{\mathrm{deg}}$ is replaced by the deterministic battery degradation coefficient $5.24 \times 10^{-4}$.

We implemented the convex relaxation of our model in Julia using CPLEX 12.7.1 and SDDP.jl [18]. Implementing

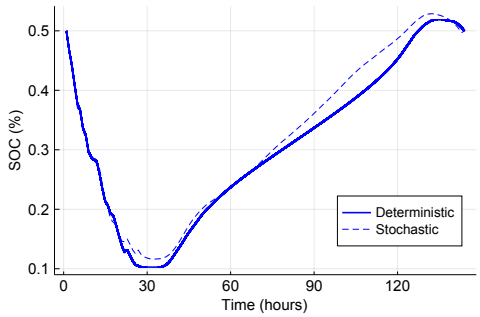


Fig. 3. Comparison of SOC trajectories using the deterministic degradation coefficient versus the stochastic degradation coefficient. The trajectories are the averages over 200 simulated cases.

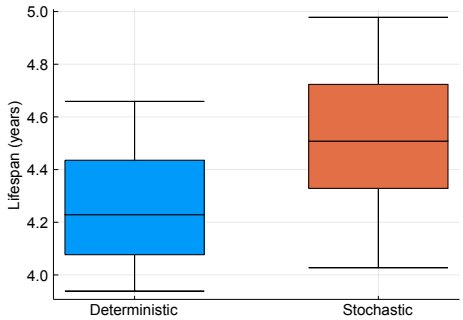


Fig. 4. Comparison of battery lifespan using the deterministic degradation coefficient versus the stochastic degradation coefficient based on 200 simulated cases.

TABLE II
RESULTS COMPARISON BETWEEN FORMULATIONS

| | Deterministic | Stochastic | % Difference |
|---|---|---|---|
| Total PV curtailed (%) | 21.19 | 21.38 | 0.89% |
| Total power for FR (kW) | 3199 | 4149 | 25.9% |
| Total power for sale (kW) | 54401 | 53451 | 1.76% |
| FR fraction of services (%) | 5.55 | 7.20 | 25.9% |

the policy derived from SDDP, we simulated 200 cases with the same stochastic variable sets used to develop the policy.

### A. Results

The average SOC trajectories over 200 simulated cases for both the deterministic and stochastic degradation formulations are shown in Fig. 3. The total percentage of PV curtailed, the sum of all the power allocated for FR and for sale to the grid, as well as the fraction of total allocated power devoted to FR over the 12-hour horizon for both formulations are given in Table II. The percent difference between the two formulations for all quantities is also given for comparison. The figure shows that the policy derived with the stochastic degradation model typically results in slightly more conservative use of the battery.

The more conservative BESS charging and discharging scheme can be attributed to the risk of higher levels of degradation in the stochastic model accounted for by the $\text{CVaR}_\alpha$. For the deterministic degradation model, a decision to charge or discharge the BESS has a known cost. For the stochastic degradation model, there is a risk that the degradation cost could be greater than the cost assumed by the deterministic model. The effective expected degradation cost in the problem is the weighted sum of the expected cost of degradation and the expected cost of the $\alpha$-fraction of most expensive degradation. The effective expected degradation cost for the deterministic degradation model is equivalent to the expected cost, as there is no risk of more expensive degradation. The effective expected cost of degradation is greater in the stochastic degradation case because the risk of more expensive degradation exists.

Degradation is modeled as a function of power entering and leaving the BESS, so minimizing that power transaction minimizes the effective expected degradation cost. However, using the BESS can result in revenue that may outweigh the cost of degradation. Revenue can result from selling excess PV power, selling power from the BESS, or using power from the BESS to provide FR. This first choice leads to no degradation of the BESS, but is only an option if there is more than sufficient power output from the PV to meet the demand of the flexible load. The other two choices can be made anytime there is sufficient charge left in the BESS (and sufficient room for charge in the FR case), but come at the cost of degradation. Selling power to the grid from the BESS guarantees that the amount of power allocated for sale will be discharged, corresponding to a known reimbursement and known input to the degradation cost function. Choosing to allocate BESS power to FR will result in a known reimbursement, since payment is only dependent on allocated capacity. The actual power actuation to provide FR will be some positive or negative value of less than or equal in magnitude to the allocated capacity (positive meaning $p^d > 0$ and negative meaning $p^c > 0$). Therefore, it is likely that the input to the degradation cost function will be less than it would be for the same allocation of power to selling to the grid. This suggests that FR provides a lower risk of degradation. Combining this with the fact that effective expected degradation cost is higher for the stochastic degradation formulation suggests that providing FR may be cost effective for the stochastic degradation formulation more often than it is for the deterministic degradation formulation. This explains the higher allocation to FR in the stochastic degradation model formulation. We note that this result might seem counter-intuitive; anecdotally batteries providing FR tend to degrade quickly. However, the alternative here – using the battery to transact energy every 5 minutes – can degrade the battery even faster since the battery can experience more/deeper SOC cycles, which determine degradation in the model in [9].

How much greater the effective expected cost for the stochastic case is in comparison to the deterministic case is dependent on the range of $\Omega^{\text{deg}}$. A wider range, meaning the most expensive degradation is further from the average, leads to a larger discrepancy between the two effective expected costs. This is because the risk of expensive degradation increases and so the expected cost of the $\alpha$-fraction of most expensive degradation also increases.

To quantify the affects of using a stochastic degradation model in terms of battery capacity loss and lifespan, capacity

loss over the 12-hour operating period was calculated using the rainflow counting method and the operating data for the 200 simulations for both formulations. For fair comparison, the deterministic stress function was used for both formulations. The magnitude of degradation from the 12-hour operation was very small for both formulations, but the stochastic degradation model resulted in about 4.80% less degradation on average. Assuming the the BESS repeatedly operates the 12-hour trajectory until reaching EOL, Fig. 4 shows the spread of battery lifespans resulting from the operating policies of the 200 simulated cases. On average, using the stochastic degradation model results in a lifespan of 4.51 years, compared to 4.25 years with the deterministic degradation model.

Including the stochastic degradation coefficient leads to a significantly longer solve time, taking 44.92 hours for 20 iterations compared to 2.04 hours for the deterministic coefficient formulation to solve with the same number of iterations using a 64-bit Intel i7-6700 core CPU at 3.40 GHz and 16-GB RAM. In practice it would be necessary to solve this problem every 12 hours, or ideally as frequently as predictions can be updated. Clearly the solve time for the formulation with the stochastic degradation model prevents practical use, as it is currently implemented. Future work could explore more efficient implementations and/or parallelization. While the solve times between the two formulations was drastically different, the number of iterations of the SDDP algorithm needed for convergence was about the same.

Very small levels of simultaneous charging and discharging occurred in the solution, likely resulting from numerical error. This suggests that the relaxation permitting simultaneous charging and discharging had insignificant impact on the results for our specific formulation and parameter set.

## V. Conclusion

In this paper, we explored the impact of using a stochastic degradation model to optimize the operation of a BESS providing grid services. The case study results showed that using a stochastic degradation model leads to a more conservative BESS charging and discharging scheme compared to using a deterministic degradation model. The more conservative operation would lead to an extension of the BESS's usable life by about 1.5% on average. The risk of more expensive degradation resulted in a policy where the system allocated more power capacity to frequency regulation and less to selling to the grid. The computation time required to compute a SDDP policy for the formulation with the stochastic degradation model was over 22 times greater than the computation time required for the formulation with a deterministic degradation model and beyond the solve time needed for practical use. How the choice of $\beta$ and $\alpha$ values affects the variation in policies as well as how to determine a suitable $\Omega^{\text{deg}}$ will be explored in future work. Additional future work includes altering the formulation and/or implementation to improve computational efficiency and practicality.


## Acknowledgments

We thank Prof. Bolun Xu for his incredibly helpful responses to our questions about the battery model in [9].


## References


[1] Y. Shi, B. Xu, D. Wang, and B. Zhang, "Using battery storage for peak shaving and frequency regulation: Joint optimization for superlinear gains," *IEEE Transactions on Power Systems*, vol. 33, no. 3, pp. 2882–2894, 2017.

[2] X. Jin, A. Vora, V. Hoshing, T. Saha, G. Shaver, O. Wasynczuk, and S. Varigonda, "Applicability of available Li-ion battery degradation models for system and control algorithm design," *Control Engineering Practice*, vol. 71, pp. 1–9, 2018.

[3] A. Maheshwari, N. G. Paterakis, M. Santarelli, and M. Gibescu, "Optimizing the operation of energy storage using a non-linear lithium-ion battery degradation model," *Applied Energy*, vol. 261, p. 114360, 2020.

[4] D. M. Rosewater, D. A. Copp, T. A. Nguyen, R. H. Byrne, and S. Santoso, "Battery energy storage models for optimal control," *IEEE Access*, vol. 7, pp. 178 357–178 391, 2019.

[5] B. Xu, A. Oudalov, A. Ulbig, G. Andersson, and D. S. Kirschen, "Modeling of lithium-ion battery degradation for cell life assessment," *IEEE Transactions on Smart Grid*, vol. 9, no. 2, pp. 1131–1140, 2018.

[6] F. Yang, D. Wang, Y. Xing, and K.-L. Tsui, "Prognostics of li(nimnco)o2-based lithium-ion batteries using a novel battery degradation model," *Microelectronics Reliability*, vol. 70, pp. 70–78, 2017.

[7] A. J. Conejo, M. Carrión, and J. M. Morales, *Risk management*. Springer, 2010, pp. 121–156.

[8] L. Herre, J. L. Mathieu, and L. Söder, "Impact of market timing on the profit of a risk-averse load aggregator," *IEEE Transactions on Power Systems*, vol. 35, no. 5, pp. 3970–3980, 2020.

[9] B. Xu, J. Zhao, T. Zheng, E. Litvinov, and D. S. Kirschen, "Factoring the cycle aging cost of batteries participating in electricity markets," *IEEE Transactions on Power Systems*, vol. 33, no. 2, pp. 2248–2259, 2018.

[10] D.-I. Stroe, M. Swierczynski, A.-I. Stroe, R. Teodorescu, R. Laerke, and P. C. Kjaer, "Degradation behaviour of lithium-ion batteries based on field measured frequency regulation mission profile," in *IEEE Energy Conversion Congress and Exposition*, 2015, pp. 14–21.

[11] O. Mégel, J. L. Mathieu, and G. Andersson, "Stochastic dual dynamic programming to schedule energy storage units providing multiple services," in *IEEE PowerTech*. IEEE, 2015.

[12] P. Fortenbacher, J. L. Mathieu, and G. Andersson, "Modeling, identification, and optimal control of batteries for power system applications," in *Power Systems Computation Conference*, 2014.

[13] D.-I. Stroe, M. Świerczyński, A.-I. Stan, R. Teodorescu, and S. J. Andreasen, "Accelerated lifetime testing methodology for lifetime estimation of lithium-ion batteries used in augmented wind power plants," *IEEE Transactions on Industry Applications*, vol. 50, no. 6, pp. 4006–4017, 2014.

[14] P. Aaslid, M. M. Belsnes, and O. B. Fosso, "Optimal microgrid operation considering battery degradation using stochastic dual dynamic programming," in *International Conference on Smart Energy Systems and Technologies*, 2019.

[15] PJM, "RTO regulation signal data for 7.2020," 2020.

[16] M. V. Pereira and L. M. Pinto, "Multi-stage stochastic optimization applied to energy planning," *Mathematical programming*, vol. 52, no. 1, pp. 359–375, 1991.

[17] J. Zou, S. Ahmed, and X. A. Sun, "Stochastic dual dynamic integer programming," *Mathematical Programming*, vol. 175, no. 1, pp. 461–502, 2019.

[18] O. Dowson and L. Kapelevich, "SDDP.jl: a Julia package for stochastic dual dynamic programming," *INFORMS Journal on Computing*, no. 1, pp. 27–33, 2021.

[19] G. He, Q. Chen, C. Kang, P. Pinson, and Q. Xia, "Optimal bidding strategy of battery storage in power markets considering performance-based regulation and battery cycle life," *IEEE Transactions on Smart Grid*, vol. 7, no. 5, pp. 2359–2367, 2016.

[20] I. Laresgoiti, S. Käbitz, M. Ecker, and D. U. Sauer, "Modeling mechanical degradation in lithium ion batteries during cycling: Solid electrolyte interphase fracture," *Journal of Power Sources*, vol. 300, pp. 112–122, 2015.

[21] NREL, "Solar power data for integration studies- michigan," 2006.